Behavioral/Systems/Cognitive

Stimulus-Induced Changes in Blood Flow and 2-Deoxyglucose Uptake Dissociate in Ipsilateral Somatosensory Cortex

Anna Devor,[1,4,5] Elizabeth M. C. Hillman,[1] Peifang Tian,[4] Christian Waeber,[2] Ivan C. Teng,[4] Lana Ruvinskaya,[1] Mark H. Shalinsky,[1] Haihao Zhu,[3] Robert H. Haslinger,[1] Suresh N. Narayanan,[1] Istvan Ulbert,[1,7,8] Andrew K. Dunn,[9] Eng H. Lo,[3] Bruce R. Rosen,[1] Anders M. Dale,[4,5] David Kleinfeld,[6] and David A. Boas[1]

[1]Martinos Center for Biomedical Imaging, [2]Stroke and Neurovascular Regulation Laboratory, and [3]Department of Radiology, Massachusetts General Hospital, Harvard Medical School, Charlestown, Massachusetts 02129, Departments of [4]Neurosciences, [5]Radiology, and [6]Physics, University of California, San Diego, La Jolla, California 92093, [7]Institute for Psychology, Hungarian Academy of Sciences, Budapest 1068, Hungary, [8]Department of Information Technology, Peter Pazmany Catholic University, Budapest 1083, Hungary, and [9]Department of Biomedical Engineering, University of Texas at Austin, Austin, Texas 78712

The present study addresses the relationship between blood flow and glucose consumption in rat primary somatosensory cortex (SI) *in vivo*. We examined bilateral neuronal and hemodynamic changes and 2-deoxyglucose (2DG) uptake, as measured by autoradiography, in response to unilateral forepaw stimulation. In contrast to the contralateral forepaw area, where neuronal activity, blood oxygenation/flow and 2DG uptake increased in unison, we observed, in the ipsilateral SI, a blood oxygenation/flow decrease and arteriolar vasoconstriction in the presence of increased 2DG uptake. Laminar electrophysiological recordings revealed an increase in ipsilateral spiking consistent with the observed increase in 2DG uptake. The vasoconstriction and the decrease in blood flow in the presence of an increase in 2DG uptake in the ipsilateral SI contradict the prominent metabolic hypothesis regarding the regulation of cerebral blood flow, which postulates that the state of neuroglial energy consumption determines the regional blood flow through the production of vasoactive metabolites. We propose that other factors, such as neuronal (and glial) release of messenger molecules, might play a dominant role in the regulation of blood flow *in vivo* in response to a physiological stimulus.

Key words: **blood flow; cerebral cortex; corpus callosum; glucose consumption; inhibition; metabolism**

Introduction

In recent years, increasing numbers of studies have used noninvasive imaging technologies such as fMRI and PET to investigate brain function. However, interpretation of these macroscopic signals in terms of the underlying microscopic neurovascular physiology is still under investigation. Theoretically, vasodilation and/or constriction can be regulated through the accumulation of energy metabolites related to neuroglial activity, the "metabolic" hypothesis; or by neuroglial release of vasoactive messengers, the "neurogenic" hypothesis (Attwell and Iadecola, 2002; Iadecola, 2004; Logothetis, 2008).

The metabolic hypothesis assumes a direct (causal) link between cellular energy state and the regulation of blood flow, possibly via astrocytic involvement (Zonta et al., 2003; Haydon and Carmignoto, 2006; Iadecola and Nedergaard, 2007; Gordon et al., 2008). The general assumption, which is supported by PET findings showing comparable functional increases in blood flow and ^{18}F-labeled 2-deoxyglucose (2DG) uptake (Fox et al., 1988; Raichle and Mintun, 2006), is that blood flow is coupled to regional glucose utilization, which in turn is directly related to neuronal activity (Magistretti, 2006). In fact, it has been argued that synaptic activity demands more metabolic energy than spiking, and for that reason is better coupled to changes in blood flow (Logothetis, 2007).

The neurogenic hypothesis (Lauritzen, 2005; Hamel, 2006) recently gained support from *in vitro* studies that demonstrated that activation of specific neuronal cell types differentially controlled the vascular response through the release of vasoactive agents (Cauli et al., 2004; Rancillac et al., 2006). *In vivo* studies have supported this hypothesis further by showing that neuronal inhibition is correlated with arteriolar vasoconstriction and a decrease in blood oxygenation known as "negative" blood oxygenation level-dependent (BOLD) response (Shmuel et al., 2006; Devor et al., 2007).

In the present study, we demonstrate a blood flow decrease and vasoconstriction, *in vivo*, in the rodent primary somatosen-

Received Sept. 9, 2008; revised Nov. 11, 2008; accepted Nov. 13, 2008.

This work was supported by National Institute of Neurological Disorders and Stroke (Grants NS-051188 to A.D., NS-057476 to D.A.B., P01NS-055104 and NS-48422 to E.H.L., NS-053684 to E.M.C.H., and NS-059832 to D.K.), National Institute of Biomedical Imaging and BioEngineering (Grants EB00790 to A.M.D., EB003832 to D.K., and EB2066 to B.R.R.), and National Center for Research Resources (Grant RR021907 to D.K.). We thank Rick Buxton for critical reading of this manuscript.

Correspondence should be addressed to Anna Devor, Martinos Center for Biomedical Imaging, Building 149, 13th Street, Mailcode 149-2301, Charlestown, MA 02129. E-mail: adevor@nmr.mgh.harvard.edu.

DOI:10.1523/JNEUROSCI.4307-08.2008

 0270-6474/08/2814347-11$15.00/0

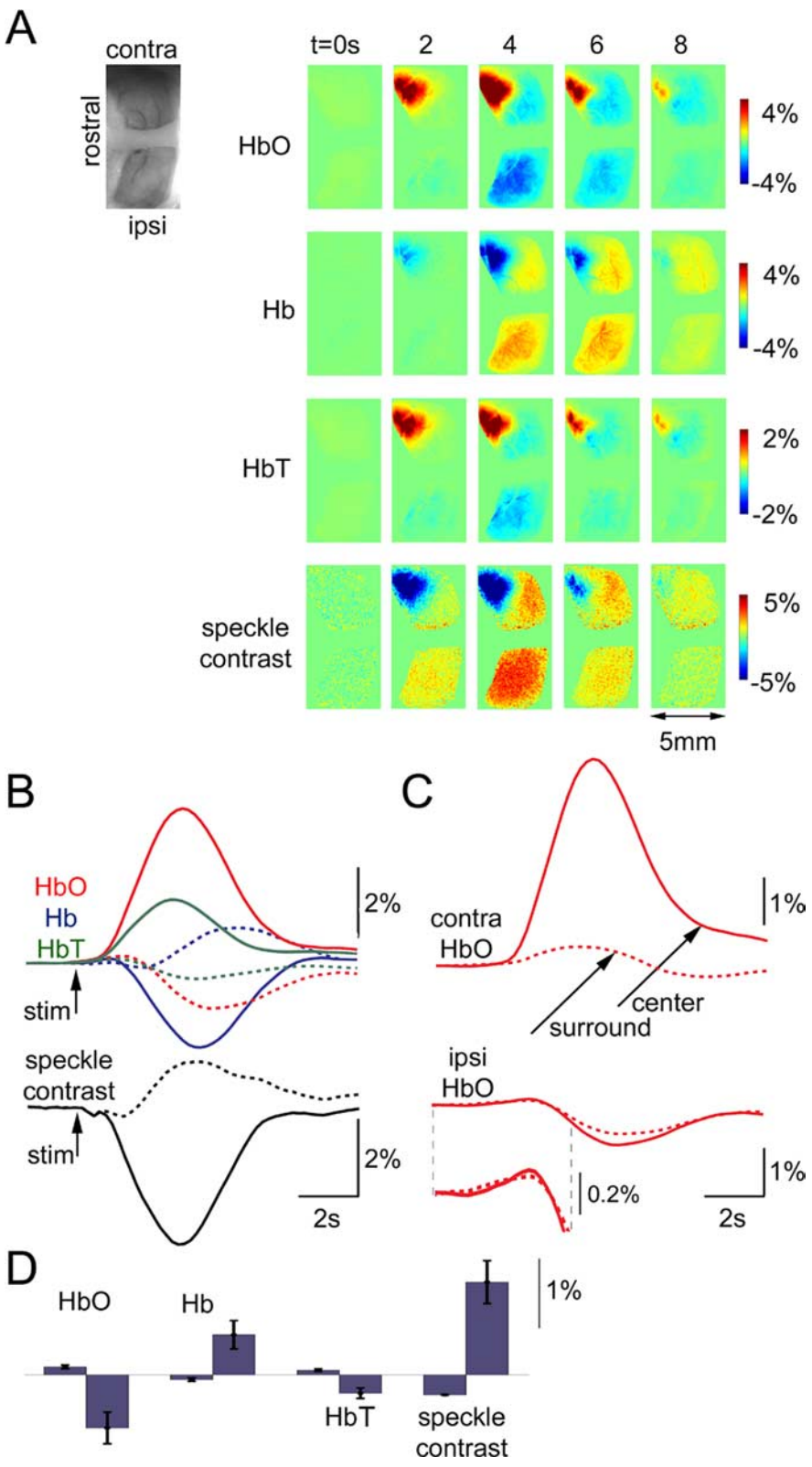

Figure 1. Bilateral hemodynamic optical imaging reveals a decrease in ipsilateral blood oxygenation and flow. ***A***, HbO, Hb, HbT, and speckle contrast images after stimulus onset ($t = 0$). The color scale is expressed as percentage signal change relative to prestimulus baseline ($\Delta C/C_0$). Time (in seconds) relative to stimulus onset is indicated above the images. One-hundred and fifty trials were averaged. We assumed baseline concentrations of 60 and 40 μM for HbO and Hb, respectively. An image of raw vasculature corresponding to functional frames is shown in the upper left corner. ***B***, Top, Signal time courses extracted from the contralateral (solid lines) and ipsilateral (dashed lines) hemispheres for HbO (red), Hb (blue) and HbT (green). Bottom, The same for speckle contrast. Note that a decrease in speckle contrast indicates an increase in blood flow. ***C***, HbO as in ***B*** broken into the center (within a 1.5 mm ring around the center of the response, solid red) and the surround (outside the 1.5 mm ring, dashed red). The center was estimated using the earliest HbT response. Contra, Contralateral to the stimulus hemisphere; ipsi, ipsilateral to the stimulus hemisphere. ***D***, Bar graphs of ΔHbO, ΔHb, ΔHbT, and Δspeckle contrast quantifying the biphasic ipsilateral response. For each measure, the first bar represents the initial (small) oxygenation/flow increase, and the second bar represents the consecutive (big) oxygenation/flow decrease. Data from five subjects were averaged. Error bars indicate SE across subjects. The following are ipsilateral mean ± SE, peaks reported in their temporal order: HbO, 0.11 ± 0.03, −0.75 ± 0.22; Hb, −0.07 ± 0.02, 0.56 ± 0.2; HbT, 0.07 ± 0.02, −0.26 ± 0.07; speckle contrast, −0.28 ± 0.01, 1.3 ± 0.2.

sory cortex (SI) in the presence of increased metabolism, as measured by 2DG autoradiography. These results suggest that factors other than metabolites of energy consumption might play a dominant role in the regulation of blood flow.

Materials and Methods

Animal preparation. Sprague Dawley rats (230–310 g) were used. Eight rats were used for spectral and speckle imaging, 10 for two-photon imaging, 22 for 2DG autoradiography and seven for laminar electrophysiological recordings. All experimental procedures were approved by the Massachusetts General Hospital Subcommittee on Research Animal Care and the University of California, San Diego Institutional Animal Care and Use Committee. Rats were initially anesthetized with isoflurane (3% initially, 1–2% during ventilation) and ventilated with a mixture of air and oxygen during surgical procedures. During the surgery, cannulas were inserted in the femoral artery and vein. Isoflurane was discontinued, and anesthesia was maintained with a 50 $mg^{*}kg^{-1}$ intravenous bolus of α-chloralose followed by continuous intravenous infusion at 40 $mg^{*}kg^{-1}{}^{*}h^{-1}$. Heart rate, blood pressure and body temperature were monitored continuously. In the majority of experiments blood gas was analyzed. With respect to respiration, we aimed to maintain $PaCO_2$ between 35 and 45 mmHg, PaO_2 between 100 and 180 mmHg, and pH between 7.35 and 7.45.

In experiments involving spectral and speckle imaging, an area of skull overlying the primary somatosensory cortex was exposed and then thinned until soft and transparent. A well of dental acrylic was built and filled with saline. In experiments involving laminar electrophysiology and two-photon microscopy, the thinned skull and dura mater were removed. To avoid herniation of the exposed brain due to excessive intracranial pressure, dura mater over the IVth cerebral ventricle was punctured and a plastic PE50 tube was inserted to allow draining of CSF. In two-photon experiments, the draining hole was sealed after sealing of the imaging well.

In tetrodotoxin (TTX) experiments, a small hole was made in the thinned bone and the underlying dura over the center of the response in one hemisphere, estimated from spectral imaging, and ~1 μl of 50 μM of TTX in artificial CSF (ACSF) was pressure-injected at a depth of 500 μm. An identical procedure was performed in

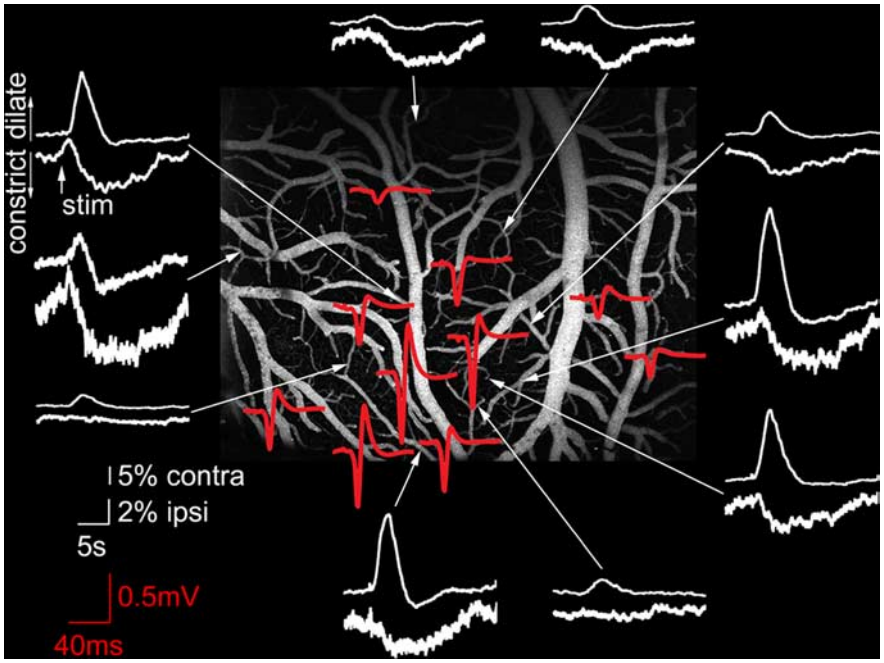

Figure 2. Arteriolar diameter change in response to contra and ipsilateral stimulation. White traces show percentage diameter change relative to the baseline ($\Delta d/d$) at different locations indicated by arrows. At every location, the upper and lower trace in a pair represents the response to the contra and ipsilateral stimulation, respectively. Dilation is plotted upward; constriction, downward. The center of the neuronal response was mapped on the cortical surface using a ball electrode. Surface potential recordings from different locations are shown in red. The strongest amplitude and fastest rise time indicate the center. The traces are overlaid on a two-photon image of vasculature within the exposure. The image was calculated as a maximum intensity projection of an image stack 0–300 μm in depth. Individual images were acquired every 10 μm. The horizontal dimension is 3.2 mm.

the opposite hemisphere, but only ACSF was injected.

The stimulation duration was 2 s and consisted of a train of six electrical pulses (3 Hz, 300 μs, 0.5–2 mA) delivered to a forepaw through a pair of thin needles implanted under the skin. The intensity was adjusted to provide stimulation below the movement threshold. For hemodynamic imaging we used either a block design with interstimulus interval (ISI) of 20 s or a rapid event-related design with 3 s ISI including 25% blank (no-stimulus) trials. Electrophysiological data were acquired using 5 s ISI to optimize for the number of trials. 2DG autoradiography experiments used the rapid event-related design (2 s of stimulation with 3 s ISI).

Spectral and laser speckle imaging of blood oxygenation and flow. Spectral imaging of blood oxygenation was performed simultaneously with laser speckle imaging of blood flow. Detected light was split via a dichroic mirror, filtered and directed toward two dedicated detectors for imaging of blood oxygenation and speckle contrast, respectively. The filtering was achieved by passing light <650 nm to the spectral detector, and 780 nm light (FWHM of 10 nm) to the speckle detector.

Spectral imaging has been described in detail previously (Dunn et al., 2003). Six different bandpass filters were placed on a six-position filter wheel (Thorlabs), which was mounted on a DC motor. The center wavelength of the filters ranged from 560 to 610 nm with 10 nm intervals. Illuminating light from a tungsten-halogen light source (Oriel, Spectra-Physics) was directed through the filter wheel, which was coupled to a 12 mm fiber bundle. Images of a ~6 × 12 mm area were acquired with a cooled 16-bit CCD camera (Cascade 512B, Photometrics). Image acquisition was triggered at ~13 Hz by individual filters in the filter wheel passing through an optical sensor. The image set at each wavelength was averaged across trials, and the averaged data were converted to changes in oxyhemoglobin (HbO) and deoxyhemoglobin (Hb) at each pixel using the modified Beer Lambert relationship: $\Delta A(\lambda,t) = (\varepsilon_{HbO}(\lambda)\Delta C_{HbO}(t) + \varepsilon_{Hb}(\lambda)\Delta C_{Hb}(t))D(\lambda)$, where $\Delta A(\lambda,t) = \log(R_o/R(t))$ is the attenuation at each wavelength, R_o and $R(t)$ are the measured reflectance intensities at baseline and time t, respectively, ΔC_{HbO} and ΔC_{Hb} are the changes in the concentrations of HbO and Hb, respectively, and ε_{HbO} and ε_{Hb} are the molar extinction coefficients. The equation was solved for ΔC_{HbO} and ΔC_{Hb} using a least-squares approach. The differential pathlength factor, $D(\lambda)$, accounts for the fact that each wavelength travels a slightly different pathlength through the tissue due to the wavelength dependence of scattering and absorption in the tissue and was estimated using the approach of Kohl et al. (2000) through Monte Carlo simulations of light propagation in tissue. Baseline concentrations of 60 and 40 μM were assumed for HbO and Hb, respectively (Mayhew et al., 2000; Jones et al., 2002).

Spectral imaging in the brain detects perfusion- and metabolism-related signals, including hemoglobin oxygenation changes, cytochrome oxidation changes, and light scattering. The hemoglobin in blood is the most significant absorber in the brain at visible wavelengths, such as within the 560–610 nm window used in this study (Frostig et al., 1990; Grinvald, 1992; Narayan et al., 1994, 1995; Malonek and Grinvald, 1996; Nemoto et al., 1999; Vanzetta and Grinvald, 1999).

A laser diode (785 nm, 80 mW) was used as a light source for speckle imaging. Raw speckle images were acquired by a high-speed (~120 Hz) 8-bit CMOS camera (A602f, Basler) with an exposure time of 5 ms and an in-plane resolution of ~20 μm. The speckle contrast is defined as the ratio of the SD to the mean pixel intensities, $\sigma/\langle I\rangle$ within a localized region of the image (Briers, 2001). Speckle contrast was calculated in a series of laser speckle images, as described in (Dunn et al., 2001, 2005) following spatial smoothing using a 5 × 5 pixel sliding window. Note that a decrease in speckle contrast indicates an increase in blood flow.

Two-photon microscopy. A chamber consisting of a metal frame (Kleinfeld and Delaney, 1996) and a removable glass coverslip lid was glued to the skull. The space between the exposed brain surface and the coverglass was filled with 0.7% (w/v) agarose (Sigma) in ACSF. To visualize the vasculature, ~0.3 ml of 5% (w/v) solution of 2 MDa fluorescein-conjugated dextran (FD-2000S, Sigma) in physiological saline was injected intravenously (Nishimura et al., 2006). The dye labeled blood plasma, while blood cells appear as dark shadows on the bright background.

Images were obtained using a home-built two-photon laser scanning microscope (Tsai et al., 2002), as described by Schaffer et al. (2006) and using an Ultima two-photon microscopy system from Prairie Technologies. We used a 4× air objective (Olympus XLFluor4×/340, NA = 0.28) to obtain images of the surface vasculature across the entire cranial window, to aid in navigating around the cortical vasculature. 10× (Zeiss Achroplan, NA = 0.3) and 20× (Olympus, NA = 0.5) water-immersion objectives were used for high-resolution imaging and line scan measurements. For diameter measurements, <500 μm-long line scans were acquired across multiple vessels (up to 6) with a scan rate of 156 Hz. The lateral scan resolution was 0.6 μm or less. One or two locations (arterioles) per animal were measured at ~1 h intervals. The data acquisition was terminated when the response amplitude at these "control" locations started to decrease, indicating a general deterioration of physiological conditions. Diving arterioles were measured in frame mode at 5–15 frames/s. Data analysis was performed in a Matlab environment.

2DG autoradiography. Sensory stimulation started either simultaneously with ($n = 8$) or 10 min before ($n = 7$) bolus injection of 0.2 ml of 2-[^{14}C(U)]-deoxy-D-glucose from Perkin-Elmer, 287 mCi/mmol and continued for 45 min. Blood samples (~0.05 ml) were collected to reconstruct the glucose and [^{14}C]2DG concentration in arterial plasma.

Forty-five minutes following the bolus injection of the tracer, the animals were killed and the brains quickly removed and frozen in −45°C isopentane. Coronal 20 μm sections were thaw-mounted on glass slides. Radioactive levels were quantified by exposing the slides and matching ^{14}C standards (calibrated for 20 μm tissue equivalents) to film (Kodak Biomax MR). We used [^{14}C]-labeled methacrylate autoradiography standards from GE Life Sciences. Local cerebral metabolic rate of glucose consumption (LCMRglu) was estimated as described by Sokoloff et al. (1977). Blood samples were collected 1 min before the tracer injection and at the following time points after the tracer injection: 15, 30, and 45 s, 1, 2, 3, 5, 10, 15, 25, and 45 min. No correction was made for the lumped constant that was assumed to be 0.48. This is in accordance with previous reports where the lumped constant was assumed to be the same in control and diabetic rats (Saker et al., 1998). The constants used were: k1 = 0.189, k2 = 0.245, k3 = 0.052. The calculation was implemented in software (MCID Elite M6; Interfocus Imaging), which yielded values for glucose consumption in each pixel. Quantitative analysis was performed in Matlab using software written in-house. Every 10 consecutive sections were averaged between AP 2.5 and −0.5 mm relative to bregma. We defined a cortical region of interest as follows: we traced the cortical surface along the dorsal curvature of the brain surface, from the medial ridge to the most lateral point of the hemisphere (where the horizontal dimension of the brain is the widest). The curvature was divided into 20 equal segments. At the border of each segment a line was drawn perpendicular to the surface throughout the cortical depth. The depth was adjusted to follow lateral gray/white matter boundary for each section. The deep ends were connected, creating 20 sectors that divided the dorsal half of cortex. The same procedure was performed for the right and left hemispheres. The metabolic rate of glucose in each sector was calculated as a mean of all pixels.

2DG autoradiography is an accumulative method and the accumulation of label occurs over 45 min. The stimulation that was presented during these 45 min was identical in all parameters (including the duty cycle) to that used in spectral/speckle measurements. No attempt was made to quantitatively compare flow and glucose consumption, only the sign (increase or decrease from the baseline).

Electrophysiological recordings. Extracellular microelectrodes (2–4 MΩ, FHC) were used to map the location of maximal neuronal response to the contralateral stimulation. The focus of activity was determined by listening to the audio signal (spikes) in response to the stimulation. Following this, the electrode was withdrawn and replaced by a linear multielectrode array with 24 contacts spaced at 100 μm (Ulbert et al., 2001). Laminar profiles of multiple unit activity (MUA) were recorded from a single location: the center of the activity in response to the contralateral stimulation. The depth was estimated based on a contact number when contact #1 was positioned at the cortical surface using visual control. The signals were amplified and filtered between 500 and 5000 Hz to record MUA. The MUA signals were rectified on the time axis before averaging.

Surface potentials recordings were conducted before 2-photon imaging using a surface silver ball electrode. Ball electrode recordings were performed from 10 to 15 locations within a ~6 × 6 mm exposure of the recording/imaging chamber. The electrode was positioned in direct contact with the cortical surface. The surface was kept moist with repeated application of ACSF. The recording locations were registered relative to the cortical microvasculature for comparison with the two-photon data. The signals were amplified and filtered between 0.1 Hz and 10 kHz.

Results

In our previous study in the rat SI, we demonstrated that vasoconstriction and a decrease in blood oxygenation correlate with neuronal inhibition (Devor et al., 2007). The present study addresses the relationship between blood flow and glucose consumption, as measured by 2DG autoradiography under vasoconstriction evoked by somatosensory stimulation. In particular, to avoid a potential cross talk between the 2DG signals in neighboring cortical areas, we take advantage of the previously described negative BOLD response induced by transcallosal inputs (Ferbert et al., 1992; Hlushchuk and Hari, 2006). We examine bilateral neuronal and hemodynamic changes as well as 2DG uptake in response to unilateral forepaw stimulation. Our main finding is that, despite the negative changes in blood oxygenation/flow and vasoconstriction in the ipsilateral SI, we observed an increase in metabolism, measured by 2DG uptake. The increasing metabolism was consistent with an increase in ipsilateral spiking revealed by laminar electrophysiological recordings. Together, these re-

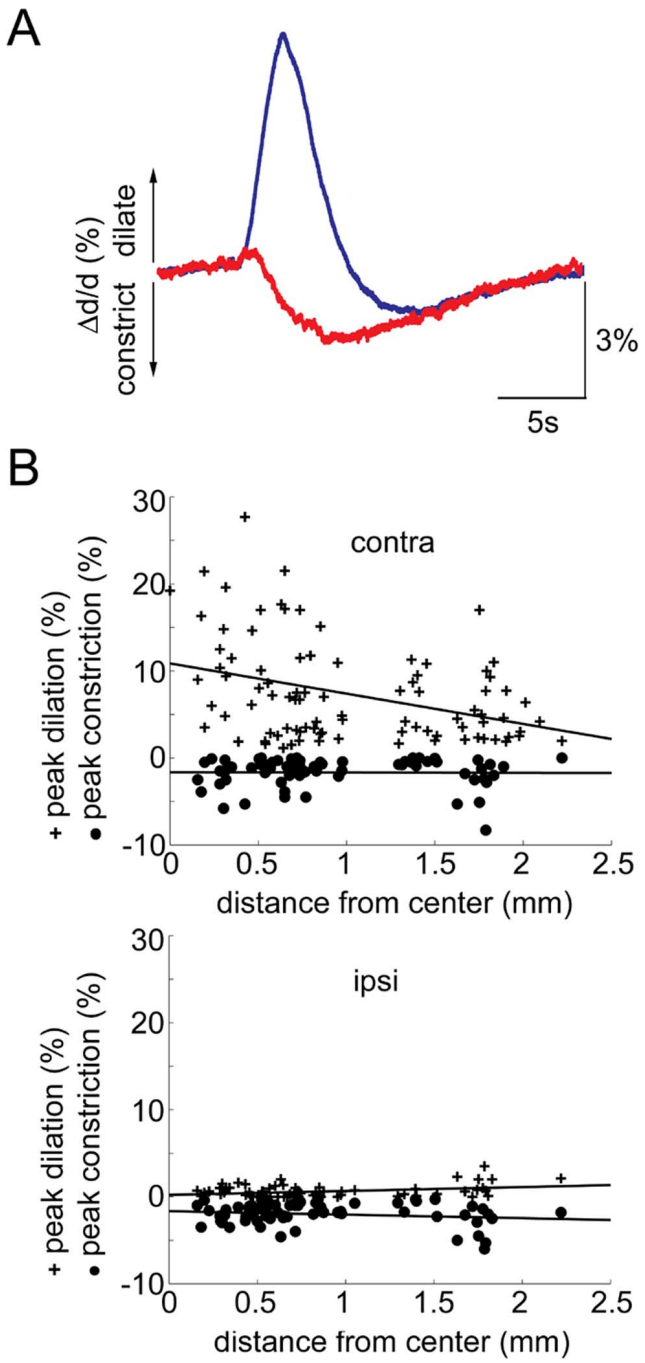

Figure 3. Comparison of arteriolar dilatation and constriction in response to contra- and ipsilateral stimulation. ***A***, An average of arteriolar diameter changes ($\Delta d/d$) in response to contralateral stimulation (blue) and ipsilateral stimulation (red). All measured vessels from all subjects are averaged. Dilation and constriction are plotted upward and downward, respectively. ***B***, Peak dilation (crosses) and peak constriction (circles) as a function of distance (in micrometers from the center of evoked neuronal response) in response to contralateral stimulation (top) and ipsilateral stimulation (bottom). Each dot represents a measurement from a single arteriole. Data from seven subjects are superimposed.

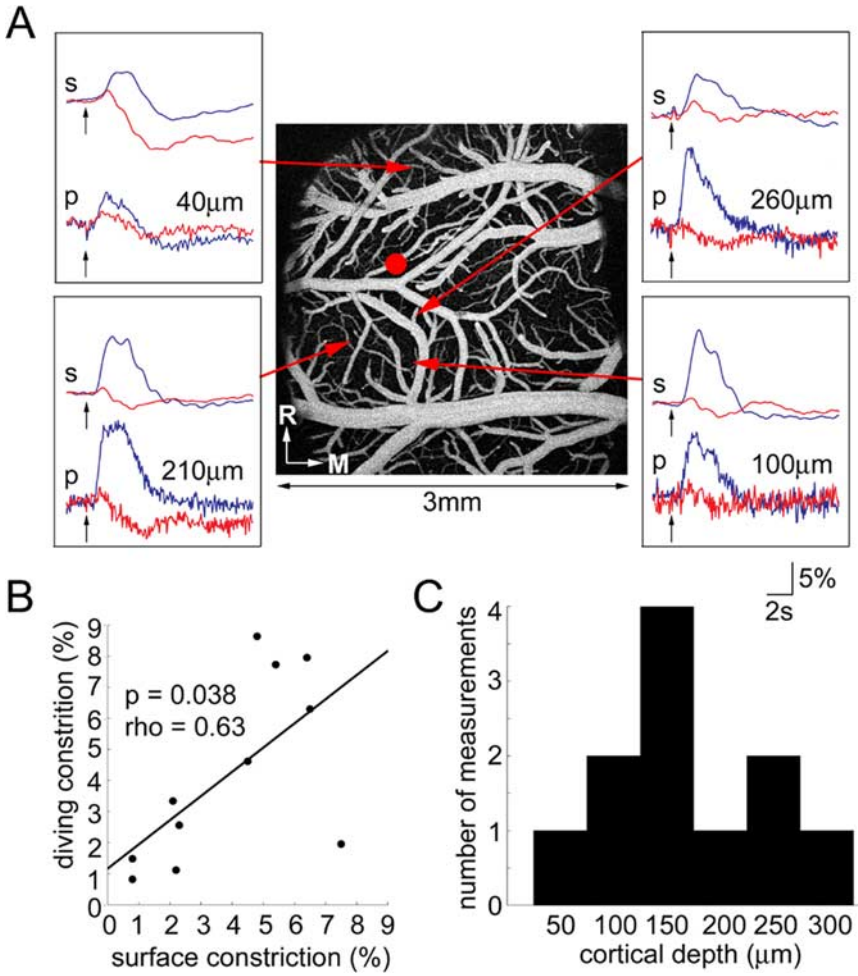

Figure 4. Comparison of surface and diving arterioles. ***A***, Diameter changes ($\Delta d/d$) in response to contralateral stimulation (blue) and ipsilateral stimulation (red) at four locations were measured in one subject. At every location, the measurement was made from a parent surface arteriole (s, top pair of traces) and a penetrating (diving) arteriole (p, bottom pair of traces). Dilation and constriction are plotted upward and downward, respectively. Black arrows indicate stimulus onset. Red arrows point to the specific surface arterioles from which the measurements were made. The red circle shows the center of neuronal response. Depth (in μm) is indicated next to each penetrating arteriole. The image of the vasculature was calculated as a maximum intensity projection of an image stack 0–300 μm in depth. Individual images were acquired every 10 μm. ***B***, Peak ipsilateral constriction of diving arterioles as a function of that of a parent surface branch. Amplitude was normalized using dilation in response to the contralateral stimulation. Data from three subjects are superimposed. ***C***, Depth distribution of the measured diving arterioles.

sults indicate a surprising inverse relationship between the metabolic rate of glucose consumption and blood oxygenation/flow that is hard to reconcile with the metabolic hypothesis.

Decreases in blood oxygenation and flow are observed in ipsilateral SI

We performed spectral imaging of oxyhemoglobin (HbO), deoxyhemoglobin (Hb) and total hemoglobin (HbT) simultaneously with laser speckle imaging of blood flow to image bilateral cortical hemodynamic responses to unilateral forepaw stimulation. We used two groups of animals: the first group ($n = 3$) received stimulation with a block design; the second group ($n = 2$), with a rapid and randomized event-related design (see Materials and Methods). The response had similar characteristics in both groups, and all of the subjects are pooled in Figure 1. In all subjects, stimulation produced a large increase in blood oxygenation and flow in the forepaw area of the SI contralateral to the stimulation and a decrease in blood oxygenation and flow in the ipsilateral SI (Fig. 1*A*). Response time courses were extracted from all pixels within contralateral and ipsilateral exposure (Fig. 1*B*, solid and dashed lines, respectively). With respect to the contralateral response, all ipsilateral measures (HbO, Hb, HbT, and speckle contrast) exhibited a reversed sign. We divided each hemisphere into two regions by drawing a 1.5 mm radius ring around the center of the hemodynamic response. The center was estimated as the peak of the earliest detectable HbT change. Response time courses were averaged from all pixels within and beyond the 1.5 mm ring (Fig. 1*C*, "center" and "surround"). While the contralateral response had a center-surround pattern, as was reported previously using a shorter stimulation (Devor et al., 2007), an ipsilateral decrease in blood oxygenation and flow was observed both in the center and in the surround. Careful examination of the ipsilateral response revealed an initial small-amplitude deflection of an opposite sign (Fig. 1*C*, bottom), indicating a small but evident increase in oxygenation/flow (Fig. 1*D*). Note that a decrease in speckle contrast indicated an increase in blood flow.

Anatomical substrates for bilateral integration in the SI are provided by homotopic interconnection via the corpus callosum and (weak) ipsilateral pathways (Shuler et al., 2001). Therefore, the ipsilateral response can be mediated by commissural projection, through the ipsilateral thalamus, or both. In an additional three subjects, application of TTX to one hemisphere abolished responses to both stimulus conditions in that hemisphere, ruling out potential passive origins of the ipsilateral decrease in blood oxygenation and flow, such as blood redistribution from one hemisphere to the other (supplemental Fig. 1, available at www.jneurosci.org as supplemental material). Application of TTX to the contralateral hemisphere also abolished the response in the ipsilateral hemisphere, demonstrating that this response is mediated by commissural projections.

Arteriolar vasoconstriction underlies the ipsilateral decreases in blood flow

To tie the macroscopic observations from spectral/speckle imaging of blood oxygenation and flow to the behavior of single identified vessels, we used two-photon microscopy in conjunction with fluorescent labeling of blood plasma with fluorescein dextran (Kleinfeld et al., 1998). Evoked changes in the diameters of surface arterioles were measured in the forepaw area of the SI in response to contra and ipsilateral stimulation. Most of the measurements (94.4%) were performed on arterioles with a baseline diameter of <50 μm. The measurements were performed under the same conditions as the spectral/speckle imaging but in a different group of animals ($n = 7$). The center of forepaw cortical representation was determined by surface potentials measure-

ments (see Materials and Methods). Due to technical limitations of the two-photon microscopy setup, only one hemisphere was imaged while the stimulation alternated between the contra and ipsilateral forepaws. For each imaged arteriole ($n = 59$), the stimulation was presented sequentially to both forepaws using a block design. In addition, we imaged 33 and 10 arterioles where only contra and ipsilateral stimulation were presented, respectively. Stimulation of the contralateral forepaw produced a large-amplitude dilation followed by a small-amplitude constriction. In contrast, stimulation of the ipsilateral forepaw produced distinct vasoconstriction (Fig. 2). Of the 69 arterioles in which an ipsilateral stimulation was presented, 59 responded with predominant vasoconstriction and 10 showed no detectable response. Consistent with the observed small initial increase in ipsilateral oxygenation/flow (Fig. 1*D*), some of the responsive arterioles exhibited a small dilation preceding the constriction. Comparison of averaged contra and ipsilateral temporal response profiles further revealed distinct ipsilateral vasoconstriction (Fig. 3*A*). We measured peak dilation and constriction for each imaged arteriole (Fig. 3*B*). Following contralateral stimulation, dilation was dominant close to the center of neuronal activity and decreased with distance from the center (Fig. 3*B*, top). This finding is consistent with our previous study of the contralateral SI using a shorter stimulation (Devor et al., 2007). Ipsilateral stimulation induced mostly vasoconstriction (Fig. 3*B*, bottom). Ipsilateral dilation and constriction were $0.6 \pm 0.7\%$ and $-1.9 \pm 1.2\%$, respectively (mean $\pm$ SD). There was no significant change in ipsilateral constriction as a function of distance from the center within the exposure ($\sim$3 mm).

To address potential differential behavior across cortical layers, we compared the response profiles of diving arterioles with those of their parent surface branches in an additional three subjects. Diving arterioles ($n = 11$) were imaged down to 320 μm. Figure 4*A* shows an example of four measured pairs (surface and diving arteriole) in one subject. For each arteriole, the responses to contra and ipsilateral stimulation are superimposed (blue and red traces, respectively). Figure 4*B* shows the peak ipsilateral constriction of diving arterioles as a function of that of their parent surface branches. Constriction in response to the ipsilateral stimulation was observed at all measured depths (Fig. 4*C*).

These data indicate that arteriolar vasoconstriction underlies the decrease in blood oxygenation and flow observed in the ipsilateral SI, as measured by spectral/speckle imaging (Fig. 1).

Ipsilateral vasoconstriction and a decrease in blood oxygenation/flow is accompanied by an increase in 2DG uptake

The brain utilizes glucose as the source of energy through glycolysis and oxidative phosphorylation (for review, see Raichle and Mintun, 2006). We used 2DG autoradiography to examine 2DG uptake bilaterally following stimulation of one (right) forepaw. 2DG autoradiography is an accumulative method with limited temporal resolution (see Materials and Methods). For comparison across imaging modalities, the subjects ($n = 15$) received stimulation with the same rapid event-related paradigm as was used for spectral/speckle imaging. For quantitative analysis, the cortical area from the medial ridge to the most lateral point of the hemisphere was divided into 20 equally spaced vertical sectors (see Materials and Methods). Figure 5*A* shows the sector map superimposed onto a representative coronal section. The metabolic rate of glucose was estimated by averaging pixels within each of the sectors. Figure 5*B* shows the profile of glucose consumption as a function of section number, where section 1 is the closest to the midline. Baseline was estimated from the ipsilateral hemisphere, in sections posterior to the active region, in 10 of the 15 subjects that received stimulation, as well as from seven additional subjects that went through identical procedures but did not receive stimulation. The results show a bilateral increase in glucose consumption with a small but significant increase in the ipsilateral SI ($p < 0.05$) (Fig. 5*B*, stars). The peak of the ipsilateral response was noticeably shifted toward the midline.

To address potential differential behavior across cortical layers we divided the depth axis of the sector map into four slabs (Fig. 6). No attempt was made to match the slabs to cortical layers. As expected, there was an increase in glucose consumption in all slabs in the contralateral hemisphere (Fig. 6, left column) (Tootell et al., 1988). In the ipsilateral hemisphere, a trend was visible in all layers and, when compared with the baseline at the same depth, was statistically significant in all but the surface slabs (Fig. 6, right column).

Together, these results indicate that a small but significant increase in ipsilateral 2DG uptake occurs in the presence of vasoconstriction and a decrease in blood flow and oxygenation. This finding challenges the classical view of a tight coupling between blood flow and glucose metabolism.

Laminar electrophysiological recordings demonstrate a bilateral increase in spiking

We used laminar electrode arrays to measure neuronal spiking activity throughout the cortical depth. In seven subjects, two laminar arrays were positioned bilaterally in the forepaw area of the SI to measure MUA. The position was determined by mapping the strongest spiking response to stimulation of the contralateral forepaw. MUA measurements were obtained from each of 23 recording locations aligned perpendicular to the cortical surface (Fig. 7*A*). A stimulus-evoked increase in spiking was observed bilaterally. With respect to that in the contralateral SI, the ipsilateral spiking increase was smaller, occurred mainly in infragranular layers (Petreanu et al., 2007), and showed a delay in onset (Fig. 7*B*, black arrows). However, a detectable spiking increase was observed in all layers (Fig. 7*B*,*C*).

To evaluate the involvement of the ipsilateral thalamus we inactivated the contralateral hemisphere by placing a number of KCl crystals over the forepaw area. Inactivation of the contralateral hemisphere virtually abolished the evoked ipsilateral response (data not shown), in agreement with the TTX measurements (supplemental Fig. 1, available at www.jneurosci.org as supplemental material).

The spiking increase was associated with synaptic activity, as measured with voltage-sensitive dyes (supplemental Fig. 2 and supplemental Results, available at www.jneurosci.org as supplemental material). Moreover, the focus of spiking/synaptic activity in response to the ipsilateral stimulation was shifted toward the midline, in agreement with the 2DG autoradiographs (supplemental Fig. 3, available at www.jneurosci.org as supplemental material).

Discussion

The present study provides an experimental demonstration of the dissociation between blood flow and energy metabolism. Specifically, we show that in the ipsilateral SI, arteriolar vasoconstriction and a decrease in blood oxygenation/flow are observed in the presence of increased 2DG uptake. This finding implies that the state of neuroglial energy consumption does not determine regional blood flow.

Both surface and diving arterioles exhibited vasoconstriction

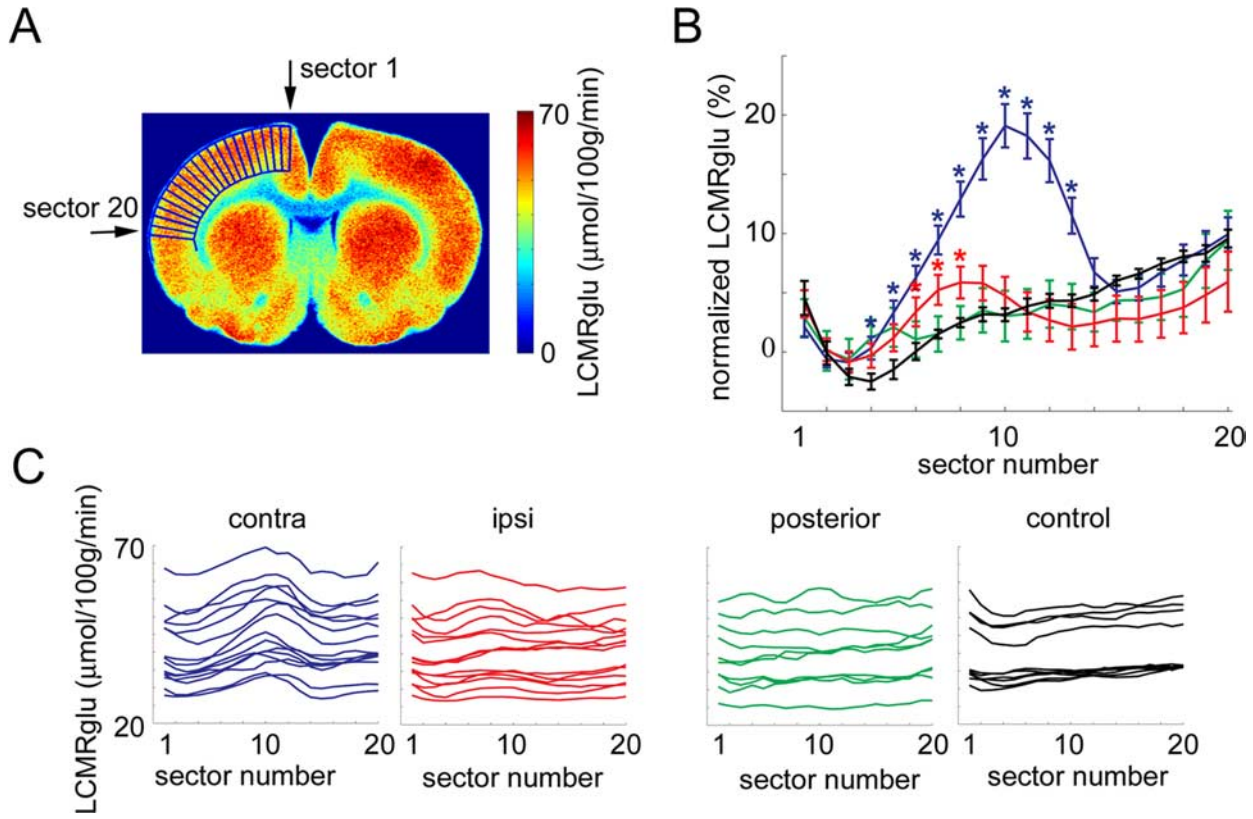

Figure 5. 2DG autoradiography in response to a unilateral stimulation. ***A***, Sector map used for quantitative analysis is overlaid on a coronal brain section. The color scale is expressed in units of local cerebral metabolic rate of glucose, LCMRglu (μmol/100 g/min). ***B***, Cortical glucose utilization profile as a function of sector number. The direction is from close to the medial ridge (sector 1) to the most lateral point of the hemisphere where the horizontal dimension of the brain is the widest (sector 20). Profiles from the contralateral (blue) and ipsilateral (red) hemispheres, posterior to the active area (green), and control subjects (no stimulus, black) are superimposed. The profiles extracted from each section have been normalized to the mean section intensity before averaging. *y*-Axis is expressed as percentage change relative to mean section intensity. Data points statistically significant from the control ($p < 0.05$) are indicated by asterisks. ***C***, Raw (not normalized) profiles extracted from the contralateral hemisphere (blue), the ipsilateral hemisphere (red), posterior to the active area (green), and control subjects (no stimulus, black). Each line represents one hemisphere. Subjects are superimposed on each plot.

in response to ipsilateral stimulation. Thus, the ipsilateral decreases in oxygenation and flow, observed with methods lacking depth resolution (Fig. 1, spectral and speckle optical imaging), likely reflect vasoconstriction (Figs. 2, 3) that occurs throughout the cortical depth (Fig. 4). A prominent constriction in response to the ipsilateral stimulation was exhibited by the majority of the arterioles examined. While some had a small-amplitude initial dilation followed by constriction, in others the response was purely constrictive. The small-amplitude initial dilation observed in some of the ipsilaterally stimulated arterioles resembles the biphasic nature of the distant contralateral surround response (see Devor et al., 2007, their Fig. 6*A*). The biphasic behavior of arteriolar diameter change in both the contra and ipsilateral hemispheres would be consistent with a "push/pull" hypothesis in which simultaneously released dilatory and constrictive agents compete as antagonistic forces, with their strengths proportional to the number of released molecules.

The small amplitude of the ipsilateral 2DG signals prevented precise laminar analysis (Fig. 5). Nevertheless, division of the cortical surface into four horizontal slabs revealed a significant ipsilateral increase in glucose consumption in all except the surface slab, with respect to the baseline at the same depth (Fig. 6). The lack of significance of the surface slab is most likely attributable to an insufficient signal-to-noise ratio in our measurement. Indeed, Using a stronger stimulation, direct cortical electrical stimulation, Weber et al. (2002) showed an increase in glucose utilization in the other hemisphere (activated through transcallosal inputs), both in layer V and in layers I–III (their Fig. 1). Dissociation between blood flow and glucose utilization has been previously reported using pharmacological approaches (Cholet et al., 1997; Vaucher et al., 1997).

The relatively low levels of baseline glucose metabolism observed in our study (<50 μmol/100 g/min) are consistent with previous reports in anesthetized rats (Nakao et al., 2001; Weber et al., 2002). In particular, Nakao et al. (2001) conducted a detailed comparative 2DG study in awake and α-chloralose-anesthetized rats and concluded that anesthesia had a prominent effect on the 2DG level. Weber et al. (2002), also using α-chloralose anesthesia, reported 40–50 μmol/100 g/min in the gray matter (their Fig. 2). Evoked increases in 2DG uptake depend not only on anesthesia conditions but also on stimulation strength and duty cycle. Ueki et al. (1992) reported a focal increase of 73 μmol/100 g/min using continuous forepaw stimulation at 3 Hz.

2DG autoradiographs (Fig. 5) and mapping of the underlying neuronal activity by voltage-sensitive dyes imaging and electrophysiological recordings (supplemental Figs. 2–3, available at www.jneurosci.org as supplemental material) indicate a shift of the center of the response toward the midline. Early tracing studies reported that commissural projections terminate in both homo and heterotopic areas in the contralateral cortex (Wise and Jones, 1976; White and DeAmicis, 1977; Ivy et al., 1979). Recently, a refinement in labeling and imaging technology allowed simultaneous *in vivo* visualization of commissural connections across multiple cortical areas (Wang et al., 2007). This study showed that in the SI (and V1) the

projections were largely restricted to borders between different subareas (e.g., to septa separating barrels in the barrel cortex). Therefore, the shift of the ipsilateral activation toward the midline might indicate a higher density of commissural projections to the border region between forepaw and hindpaw cortical representations. In addition, the larger lateral spread of the contralateral response might reflect propagation to other cortical areas and toward the SII (White and DeAmicis, 1977; Koralek et al., 1990).

The relative contributions of oxidative phosphorylation and glycolysis to the observed ipsilateral increase in glucose metabolism cannot be ascertained from our study. Since all commissural projections are glutamatergic, the observed ipsilateral increase in 2DG uptake is consistent with the work of Magistretti and colleagues (Magistretti and Pellerin, 1999; Magistretti et al., 1999; Shulman et al., 2002, 2004), and is likely to reflect, at least in part, astrocytic glycolysis (Magistretti, 2006) associated with glutamate recycling at the synapse. There is substantial evidence from other studies that, in parallel to the increased metabolism, glutamate receptor binding on the astrocyte initiates a calcium increase which in turn triggers the release of vasoactive agents that increase blood flow. However, our primary experimental finding of the conjunction of increased 2DG uptake with reduced blood flow in ipsilateral SI presents an important exception to this pattern. One possibility is that increased astrocyte activity in this case leads to a vasoconstriction signal. Recent studies, primarily with *in vitro* preparations, have found conflicting results on whether the vasoactive result is a constriction or a dilation (Zonta et al., 2003; Mulligan and MacVicar, 2004; Haydon and Carmignoto, 2006; Metea and Newman, 2006; Takano et al., 2006; Iadecola and Nedergaard, 2007), possibly depending on the baseline conditions (Blanco et al., 2008; Gordon et al., 2008). Astrocytes have also been implicated in the generation of spectral imaging signals *in vivo* (Gurden et al., 2006; Schummers et al., 2008), and *in vivo* uncaging of calcium in astrocytic endfeet has been shown to produce mostly dilation (Takano et al., 2006). A recent report based on brain slice experiments showed evidence that the tissue oxygenation affects the pathways that are activated, with increased calcium in the astrocyte initiating a chain of events that produces a vasodilation when tissue oxygenation is low and a constriction when the oxygenation is high (Gordon et al., 2008). Future tissue oxygenation measures with a similar experimental model to ours would help to determine whether such effects are important for explaining the current *in vivo* results.

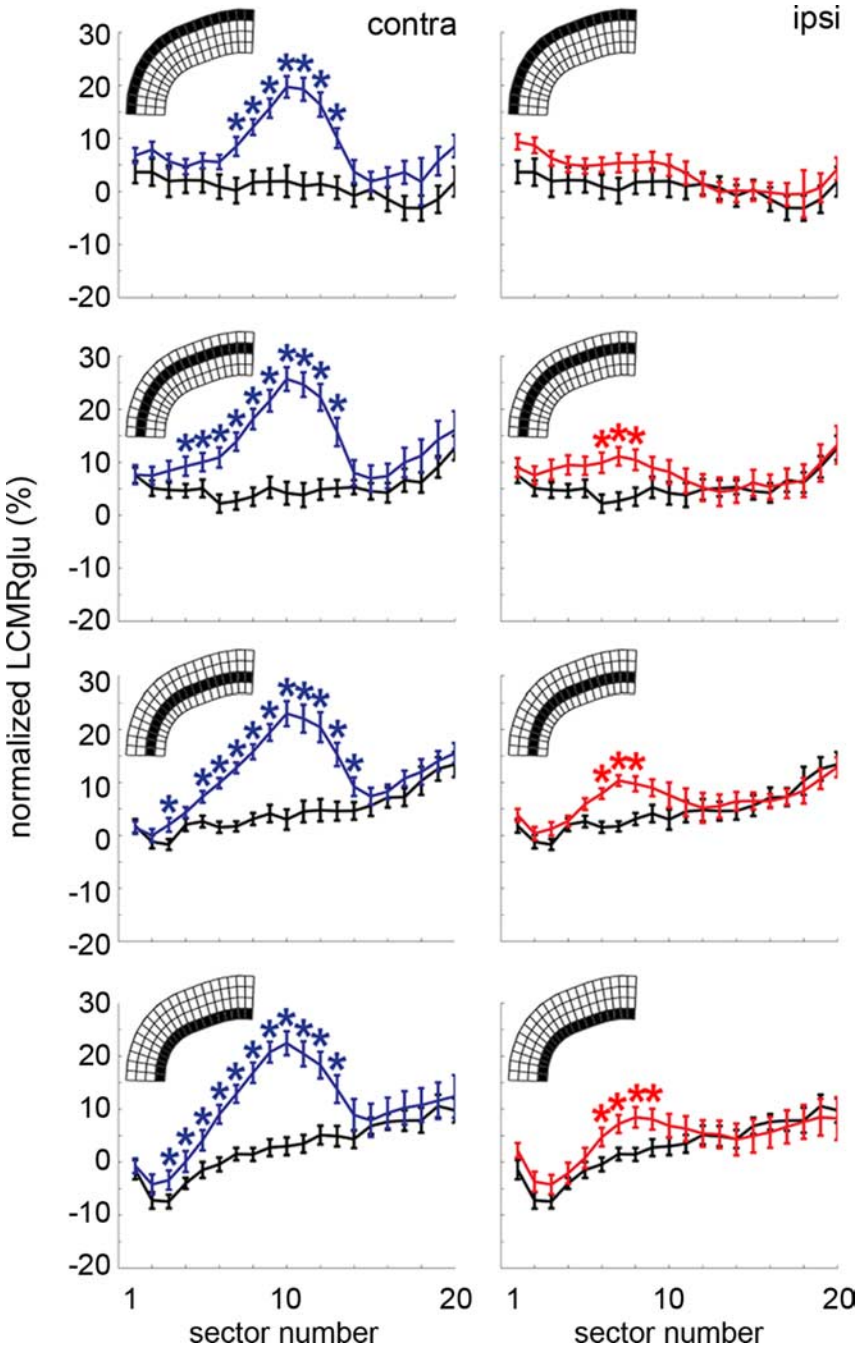

Figure 6. Laminar distribution of glucose uptake. A cortical glucose utilization profile is shown as a function of sector number in the contralateral hemisphere (left column, blue) and the ipsilateral hemisphere (right column, red). The depth axis of the sector map was divided into four slabs. Each one of the plots shows the profiles extracted from one of the slabs schematically shown in the top left corner. Each data point within a profile was calculated by averaging pixels within each of the sectors in the corresponding slab. Profiles are superimposed onto the baseline at the same depth estimated from the region posterior to the active area (black). The direction of *x*-axis is as in Figure 5: from close to the medial ridge (sector 1) to the most lateral point of the hemisphere where the horizontal dimension of the brain is the widest (sector 20). The profiles extracted from each section have been normalized to the mean section intensity before averaging. *y*-Axis is expressed as percentage change relative to mean section intensity. Data points statistically significant from the control ($p < 0.05$) are indicated by asterisks.

Repolarization following synaptic activity involves activation of Na^+/K^+ ATPase and requires energy. Therefore, both spiking and synaptic neuronal activity in the ipsilateral SI are likely to contribute to the observed increase in ipsilateral glucose utilization (Attwell and Laughlin, 2001; Attwell and Iadecola, 2002). The glutamatergic commissural projections to the ipsilateral SI, in particular to layer V (Fig. 7) (Petreanu et al., 2007), set up an

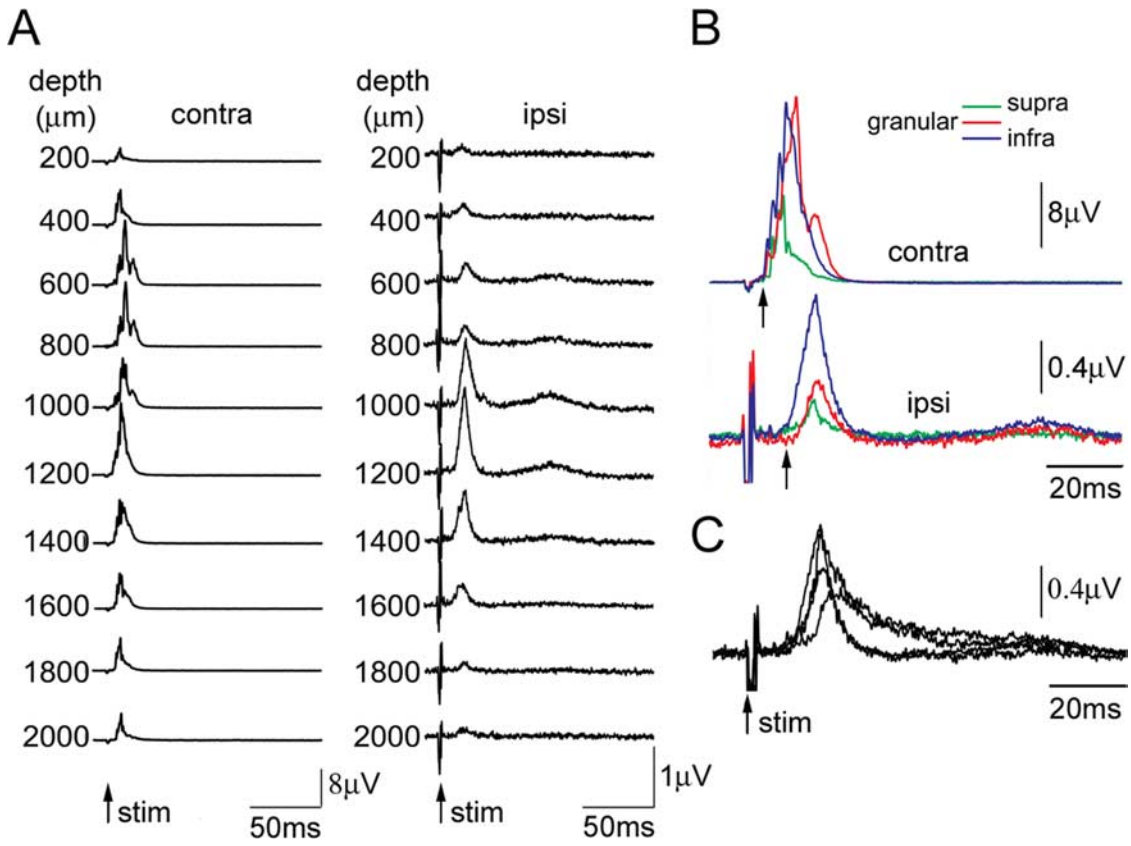

Figure 7. Laminar recordings of multiunit activity measure an increase in ipsilateral spiking. ***A***, A laminar profile of MUA response in the contralateral (left panel) and ipsilateral (right panel) hemispheres. The response to the first of the six stimuli in a train is shown. Each trace represents a recording from a single electrode in the array. The corresponding cortical depth is indicated on the left. Recordings from every other contact down to 2000 μm are shown. Five-hundred stimulation trials were averaged. Arrows denote stimulus onset. Note an increase in ipsilateral spiking. ***B***, MUA from supragranular (0–500 μm, green), granular (500–900 μm, red), and infragranular (>900 μm, blue) layers. Black arrows indicate response onset. ***C***, Infragranular MUA responses from four subjects are superimposed.

increase in the activity of local neuronal circuits, including activation of local inhibitory interneurons (supplemental Fig. 2 and supplemental Results, available at www.jneurosci.org as supplemental material) (Ferbert et al., 1992; Meyer et al., 1995; Gerloff et al., 1998; Hlushchuk and Hari, 2006). In this respect, *in vitro* studies have shown that activation of specific types of the inhibitory neurons can mediate vasoconstriction (Cauli et al., 2004; Rancillac et al., 2006). Neuronal release of vasoconstrictive messengers provides a possible explanation to our ipsilateral findings. Moreover, the release of vasoactive mediators provides an alternative explanation for the strong correlation between synaptic signal transduction and the hemodynamic response (Logothetis, 2002, 2003), which has previously been attributed to energy use (Logothetis, 2007).

Predominant inhibition is a common finding in the ipsilateral SI and the surround region in the contralateral SI (Derdikman et al., 2003; Devor et al., 2007). In this respect, the present results are consistent with our previous publication showing a correlation between surround contralateral inhibition and predominant vasoconstriction (Devor et al., 2007a,b). The present report demonstrates that the surround hemodynamic "negativity" applies also to blood flow. A sensory-evoked decrease in blood oxygenation in the ipsilateral SI has recently been reported using BOLD fMRI both in the rat whisker barrel cortex (Alonso et al., 2008) and in the human somatosensory cortex (Hlushchuk and Hari, 2006). Other fMRI studies in humans (Tootell et al., 1998; Shmuel et al., 2002; Bressler et al., 2007) and nonhuman primates (Shmuel et al., 2006) have demonstrated that negative BOLD signals are task-related and carry stimulus-specific information (Bressler et al., 2007).

The observed discrepancy between blood flow and glucose utilization further emphasizes the importance of understanding the true neurophysiological basis of noninvasive PET and fMRI neuroimaging signals. Ipsilateral dissociation between blood oxygenation/flow and glucose metabolism does not rule out the possibility that certain metabolites can have a vasoactive effect (Ido et al., 2004; Mintun et al., 2004). However, it indicates that the blood flow response is not determined by the tissue energy consumption. Other factors (e.g., release of inhibitory neuropeptides, mediated or not by astrocytes) might play a dominant role in the regulation of blood flow in the ipsilateral SI.

References

Alonso Bde C, Lowe AS, Dear JP, Lee KC, Williams SC, Finnerty GT (2008) Sensory inputs from whisking movements modify cortical whisker maps visualized with functional magnetic resonance imaging. Cereb Cortex 18:1314–1325.

Attwell D, Iadecola C (2002) The neural basis of functional brain imaging signals. Trends Neurosci 25:621–625.

Attwell D, Laughlin SB (2001) An energy budget for signaling in the grey matter of the brain. J Cereb Blood Flow Metab 21:1133–1145.

Blanco VM, Stern JE, Filosa JA (2008) Tone-dependent vascular responses to astrocyte-derived signals. Am J Physiol Heart Circ Physiol 294:H2855–H2863.

Bressler D, Spotswood N, Whitney D (2007) Negative BOLD fMRI response in the visual cortex carries precise stimulus-specific information. PLoS ONE 2:e410.

Briers JD (2001) Laser Doppler, speckle and related techniques for blood perfusion mapping and imaging. Physiol Meas 22:R35–66.

Cauli B, Tong XK, Rancillac A, Serluca N, Lambolez B, Rossier J, Hamel E (2004) Cortical GABA interneurons in neurovascular coupling: relays for subcortical vasoactive pathways. J Neurosci 24:8940–8949.

Cholet N, Seylaz J, Lacombe P, Bonvento G (1997) Local uncoupling of the cerebrovascular and metabolic responses to somatosensory stimulation after neuronal nitric oxide synthase inhibition. J Cereb Blood Flow Metab 17:1191–1201.

Derdikman D, Hildesheim R, Ahissar E, Arieli A, Grinvald A (2003) Imaging spatiotemporal dynamics of surround inhibition in the barrels somatosensory cortex. J Neurosci 23:3100–3105.

Devor A, Tian P, Nishimura N, Teng IC, Hillman EM, Narayanan SN, Ulbert I, Boas DA, Kleinfeld D, Dale AM (2007a) Suppressed neuronal activity and concurrent arteriolar vasoconstriction may explain negative blood oxygenation level-dependent signal. J Neurosci 27:4452–4459.

Devor A, Trevelyan A, Kleinfeld D (2007b) Is there a common origin to surround-inhibition as seen through electrical activity versus hemodynamic changes? Focus on "duration-dependent response in SI to vibrotactile stimulation". J Neurophysiol 97:1880–1882.

Dunn AK, Bolay H, Moskowitz MA, Boas DA (2001) Dynamic imaging of cerebral blood flow using laser speckle. J Cereb Blood Flow Metab 21:195–201.

Dunn AK, Devor A, Bolay H, Andermann ML, Moskowitz MA, Dale AM, Boas DA (2003) Simultaneous imaging of total cerebral hemoglobin concentration, oxygenation, and blood flow during functional activation. Opt Lett 28:28–30.

Dunn AK, Devor A, Dale AM, Boas DA (2005) Spatial extent of oxygen metabolism and hemodynamic changes during functional activation of the rat somatosensory cortex. Neuroimage 27:279–290.

Ferbert A, Priori A, Rothwell JC, Day BL, Colebatch JG, Marsden CD (1992) Interhemispheric inhibition of the human motor cortex. J Physiol 453:525–546.

Fox PT, Raichle ME, Mintun MA, Dence C (1988) Nonoxidative glucose consumption during focal physiologic neural activity. Science 241:462–464.

Frostig RD, Lieke EE, Ts'o DY, Grinvald A (1990) Cortical functional architecture and local coupling between neuronal activity and the microcirculation revealed by in vivo high-resolution optical imaging of intrinsic signals. Proc Natl Acad Sci U S A 87:6082–6086.

Gerloff C, Cohen LG, Floeter MK, Chen R, Corwell B, Hallett M (1998) Inhibitory influence of the ipsilateral motor cortex on responses to stimulation of the human cortex and pyramidal tract. J Physiol 510:249–259.

Gordon GR, Choi HB, Rungta RL, Ellis-Davies GC, Macvicar BA (2008) Brain metabolism dictates the polarity of astrocyte control over arterioles. Nature. Advance online publication. Retrieved December 1, 2008. doi:10.1038/nature07525

Grinvald A (1992) Optical imaging of architecture and function in the living brain sheds new light on cortical mechanisms underlying visual perception. Brain Topogr 5:71–75.

Gurden H, Uchida N, Mainen ZF (2006) Sensory-evoked intrinsic optical signals in the olfactory bulb are coupled to glutamate release and uptake. Neuron 52:335–345.

Hamel E (2006) Perivascular nerves and the regulation of cerebrovascular tone. J Appl Physiol 100:1059–1064.

Haydon PG, Carmignoto G (2006) Astrocyte control of synaptic transmission and neurovascular coupling. Physiol Rev 86:1009–1031.

Hlushchuk Y, Hari R (2006) Transient suppression of ipsilateral primary somatosensory cortex during tactile finger stimulation. J Neurosci 26:5819–5824.

Iadecola C (2004) Neurovascular regulation in the normal brain and in Alzheimer's disease. Nat Rev Neurosci 5:347–360.

Iadecola C, Nedergaard M (2007) Glial regulation of the cerebral microvasculature. Nat Neurosci 10:1369–1376.

Ido Y, Chang K, Williamson JR (2004) NADH augments blood flow in physiologically activated retina and visual cortex. Proc Natl Acad Sci U S A 101:653–658.

Ivy GO, Akers RM, Killackey HP (1979) Differential distribution of callosal projection neurons in the neonatal and adult rat. Brain Res 173:532–537.

Jones M, Berwick J, Mayhew J (2002) Changes in blood flow, oxygenation, and volume following extended stimulation of rodent barrel cortex. Neuroimage 15:474–487.

Kleinfeld D, Delaney KR (1996) Distributed representation of vibrissa movement in the upper layers of somatosensory cortex revealed with voltage-sensitive dyes. J Comp Neurol 375:89–108.

Kleinfeld D, Mitra PP, Helmchen F, Denk W (1998) Fluctuations and stimulus-induced changes in blood flow observed in individual capillaries in layers 2 through 4 of rat neocortex. Proc Natl Acad Sci U S A 95:15741–15746.

Kohl M, Lindauer U, Royl G, Kuhl M, Gold L, Villringer A, Dirnagl U (2000) Physical model for the spectroscopic analysis of cortical intrinsic optical signals. Phys Med Biol 45:3749–3764.

Koralek KA, Olavarria J, Killackey HP (1990) Areal and laminar organization of corticocortical projections in the rat somatosensory cortex. J Comp Neurol 299:133–150.

Lauritzen M (2005) Opinion: Reading vascular changes in brain imaging: is dendritic calcium the key? Nat Rev Neurosci 6:77–85.

Logothetis NK (2002) The neural basis of the blood-oxygen-level-dependent functional magnetic resonance imaging signal. Philos Trans R Soc Lond B Biol Sci 357:1003–1037.

Logothetis NK (2003) The underpinnings of the BOLD functional magnetic resonance imaging signal. J Neurosci 23:3963–3971.

Logothetis NK (2007) The ins and outs of fMRI signals. Nat Neurosci 10:1230–1232.

Logothetis NK (2008) What we can do and what we cannot do with fMRI. Nature 453:869–878.

Magistretti PJ (2006) Neuron-glia metabolic coupling and plasticity. J Exp Biol 209:2304–2311.

Magistretti PJ, Pellerin L (1999) Cellular mechanisms of brain energy metabolism and their relevance to functional brain imaging. Philos Trans R Soc Lond B Biol Sci 354:1155–1163.

Magistretti PJ, Pellerin L, Rothman DL, Shulman RG (1999) Energy on demand. Science 283:496–497.

Malonek D, Grinvald A (1996) Interactions between electrical activity and cortical microcirculation revealed by imaging spectroscopy: implications for functional brain mapping. Science 272:551–554.

Mayhew J, Johnston D, Berwick J, Jones M, Coffey P, Zheng Y (2000) Spectroscopic analysis of neural activity in brain: increased oxygen consumption following activation of barrel cortex. Neuroimage 12:664–675.

Metea MR, Newman EA (2006) Glial cells dilate and constrict blood vessels: a mechanism of neurovascular coupling. J Neurosci 26:2862–2870.

Meyer BU, Röricht S, Gräfin von Einsiedel H, Kruggel F, Weindl A (1995) Inhibitory and excitatory interhemispheric transfers between motor cortical areas in normal humans and patients with abnormalities of the corpus callosum. Brain 118:429–440.

Mintun MA, Vlassenko AG, Rundle MM, Raichle ME (2004) Increased lactate/pyruvate ratio augments blood flow in physiologically activated human brain. Proc Natl Acad Sci U S A 101:659–664.

Mulligan SJ, MacVicar BA (2004) Calcium transients in astrocyte endfeet cause cerebrovascular constrictions. Nature 431:195–199.

Nakao Y, Itoh Y, Kuang TY, Cook M, Jehle J, Sokoloff L (2001) Effects of anesthesia on functional activation of cerebral blood flow and metabolism. Proc Natl Acad Sci U S A 98:7593–7598.

Narayan SM, Santori EM, Blood AJ, Burton JS, Toga AW (1994) Imaging optical reflectance in rodent barrel and forelimb sensory cortex. Neuroimage 1:181–190.

Narayan SM, Esfahani P, Blood AJ, Sikkens L, Toga AW (1995) Functional increases in cerebral blood volume over somatosensory cortex. J Cereb Blood Flow Metab 15:754–765.

Nemoto M, Nomura Y, Sato C, Tamura M, Houkin K, Koyanagi I, Abe H (1999) Analysis of optical signals evoked by peripheral nerve stimulation in rat somatosensory cortex: dynamic changes in hemoglobin concentration and oxygenation. J Cereb Blood Flow Metab 19:246–259.

Nishimura N, Schaffer CB, Friedman B, Tsai PS, Lyden PD, Kleinfeld D (2006) Targeted insult to subsurface cortical blood vessels using ultrashort laser pulses: three models of stroke. Nat Methods 3:99–108.

Petreanu L, Huber D, Sobczyk A, Svoboda K (2007) Channelrhodopsin-2-assisted circuit mapping of long-range callosal projections. Nat Neurosci 10:663–668.

Raichle ME, Mintun MA (2006) Brain work and brain imaging. Annu Rev Neurosci 29:449–476.

Rancillac A, Rossier J, Guille M, Tong XK, Geoffroy H, Amatore C, Arbault S, Hamel E, Cauli B (2006) Glutamatergic control of microvascular tone by distinct GABA neurons in the cerebellum. J Neurosci 26:6997–7006.

Saker F, Ybarra J, Leahy P, Hanson RW, Kalhan SC, Ismail-Beigi F (1998) Glycemia-lowering effect of cobalt chloride in the diabetic rat: role of decreased gluconeogenesis. Am J Physiol 274:E984–E991.

Schaffer CB, Friedman B, Nishimura N, Schroeder LF, Tsai PS, Ebner FF, Lyden PD, Kleinfeld D (2006) Two-photon imaging of cortical surface microvessels reveals a robust redistribution in blood flow after vascular occlusion. PLoS Biol 4:e22.

Schummers J, Yu H, Sur M (2008) Tuned responses of astrocytes and their influence on hemodynamic signals in the visual cortex. Science 320:1638–1643.

Shmuel A, Yacoub E, Pfeuffer J, Van de Moortele PF, Adriany G, Hu X, Ugurbil K (2002) Sustained negative BOLD, blood flow and oxygen consumption response and its coupling to the positive response in the human brain. Neuron 36:1195–1210.

Shmuel A, Augath M, Oeltermann A, Logothetis NK (2006) Negative functional MRI response correlates with decreases in neuronal activity in monkey visual area V1. Nat Neurosci 9:569–577.

Shuler MG, Krupa DJ, Nicolelis MA (2001) Bilateral integration of whisker information in the primary somatosensory cortex of rats. J Neurosci 21:5251–5261.

Shulman RG, Hyder F, Rothman DL (2002) Biophysical basis of brain activity: implications for neuroimaging. Q Rev Biophys 35:287–325.

Shulman RG, Rothman DL, Behar KL, Hyder F (2004) Energetic basis of brain activity: implications for neuroimaging. Trends Neurosci 27:489–495.

Sokoloff L, Reivich M, Kennedy C, Des Rosiers MH, Patlak CS, Pettigrew KD, Sakurada O, Shinohara M (1977) The [14C]deoxyglucose method for the measurement of local cerebral glucose utilization: theory, procedure, and normal values in the conscious and anesthetized albino rat. J Neurochem 28:897–916.

Takano T, Tian GF, Peng W, Lou N, Libionka W, Han X, Nedergaard M (2006) Astrocyte-mediated control of cerebral blood flow. Nat Neurosci 9:260–267.

Tootell RB, Hamilton SL, Silverman MS, Switkes E (1988) Functional anatomy of macaque striate cortex. I. Ocular dominance, binocular interactions, and baseline conditions. J Neurosci 8:1500–1530.

Tootell RB, Hadjikhani N, Hall EK, Marrett S, Vanduffel W, Vaughan JT, Dale AM (1998) The retinotopy of visual spatial attention. Neuron 21:1409–1422.

Tsai PS, Nishimura N, Yoder EJ, White A, Dolnick E, Kleinfeld D (2002) Principles, design and construction of a two photon scanning microscope for in vitro and in vivo studies. In: Methods for in vivo optical imaging (Frostig RD, ed), pp 113–171. Boca Raton, FL: CRC.

Ueki M, Mies G, Hossmann KA (1992) Effect of alpha-chloralose, halothane, pentobarbital and nitrous oxide anesthesia on metabolic coupling in somatosensory cortex of rat. Acta Anaesthesiol Scand 36:318–322.

Ulbert I, Halgren E, Heit G, Karmos G (2001) Multiple microelectrode-recording system for human intracortical applications. J Neurosci Methods 106:69–79.

Vanzetta I, Grinvald A (1999) Increased cortical oxidative metabolism due to sensory stimulation: implications for functional brain imaging. Science 286:1555–1558.

Vaucher E, Borredon J, Bonvento G, Seylaz J, Lacombe P (1997) Autoradiographic evidence for flow-metabolism uncoupling during stimulation of the nucleus basalis of Meynert in the conscious rat. J Cereb Blood Flow Metab 17:686–694.

Wang Q, Gao E, Burkhalter A (2007) In vivo transcranial imaging of connections in mouse visual cortex. J Neurosci Methods 159:268–276.

Weber B, Fouad K, Burger C, Buck A (2002) White matter glucose metabolism during intracortical electrostimulation: a quantitative [(18)F]Fluorodeoxyglucose autoradiography study in the rat. Neuroimage 16:993–998.

White EL, DeAmicis RA (1977) Afferent and efferent projections of the region in mouse SmL cortex which contains the posteromedial barrel subfield. J Comp Neurol 175:455–482.

Wise SP, Jones EG (1976) The organization and postnatal development of the commissural projection of the rat somatic sensory cortex. J Comp Neurol 168:313–343.

Zonta M, Angulo MC, Gobbo S, Rosengarten B, Hossmann KA, Pozzan T, Carmignoto G (2003) Neuron-to-astrocyte signaling is central to the dynamic control of brain microcirculation. Nat Neurosci 6:43–50.